ACS OMEGA

http://pubs.acs.org/journal/acsodf

Article

Synthesis of Magnetic Short-Channel Mesoporous Silica SBA-15 Modified with a Polypyrrole/Polyaniline Copolymer for the Removal of Mercury Ions from Aqueous Solution

Jingtao Shen,[§] Shuyuan Zhang,[§] Zheng Zeng, Jialun Huang, Yi Shen, and Yongfu Guo*

Cite This: *ACS Omega* 2021, 6, 25791−25806

Read Online

ACCESS | Metrics & More | Article Recommendations | Supporting Information

ABSTRACT: A novel magnetic short-channel mesoporous silica SBA-15 composite adsorbent was prepared by the copolymerization of pyrrole and aniline. The prepared novel nanoadsorbent polypyrrole−polyaniline/$CoFe_2O_4$-SBA-15 (PPy-PANI/M-SBA-15) has a significant adsorption effect on heavy metal mercury ions. The batch adsorption experiment was carried out to study the effects of various parameters including solution pH, initial concentration (C_0), adsorbent dose (dosage), temperature (T), and contact time on the adsorption effect. The analysis results of the response surface method (RSM) and central composite design (CCD) show that the importance for adsorption factors is pH > C_0 > T > dosage, and the maximum capacity of PPy-PANI/M-SBA-15 is 346.2 mg/g under the optimal conditions of pH = 6.7, T = 310 K, C_0 = 29.5 mg/L, and a dosage of 0.044 g/L. The pseudo-second-order kinetic model and the Langmuir isotherm model simulate the adsorption behavior of mercury ions. In addition, thermodynamic parameters indicate self-heating and reversible adsorption processes. A covalent bond is formed between the nitrogen-containing functional group and the mercury ions. Excellent magnetic properties and high reproducibility indicate that PPy-PANI/M-SBA-15 has excellent recyclability and environmentally friendly properties and can become a potential heavy metal ion adsorbent in practical applications.

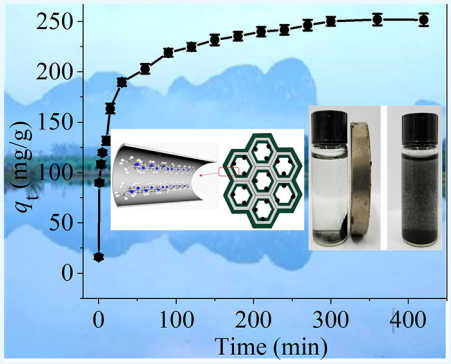

1. INTRODUCTION

In today's social life, owing to human social production activities, mercury and its compounds are widely dispersed in water bodies. It is precisely because of the widespread pollution of mercury in the environment that it is presently receiving much attention.[1] Mercury(II), as one of the main mercury species in the water phase, can combine with organic matter and inorganic matter to form a variety of complexes, which has caused a serious impact on human water bodies.[2] Mercury as a pollutant has been listed as a priority pollutant by the United Nations Environmental Protection Agency.[3] So, there is an urgent need for a technology that can effectively remove mercury from aqueous solution.

Adsorption technology, as a traditional method for treating pollutants, is relatively simple and easy to implement, and adsorbents also have a wide range of sources, such as natural resources or waste materials. So, the adsorption treatment in the removal of heavy metal ions has broad application prospects.

Ordered mesoporous molecular sieves have excellent chemical and thermal stability, high mechanical strength, and an ordered pore structure, compared to other types of heavy metal adsorbents such as clay, zeolite, and resin. Among the mesoporous molecular sieves, SBA-15 with a short pore structure has a highly ordered two-dimensional hexagonal pore structure and high stability in aqueous solution. In addition, short-channel SBA-15 is a favorable adsorbent material, which is beneficial to the diffusion of the adsorbate so as to be rapidly captured by the adsorbent.[4] However, as described in previous work, pure-silica SBA-15 has almost no adsorption capacity for Hg(II), and the SBA-15 prepared using Zr and Ce precursors only presents a relatively low adsorption capacity for Hg(II).[5,6] Furthermore, regeneration performance of SBA-15 is also an important factor restricting its application.

To solve the abovementioned problems of low adsorption capacity, polypyrrole and polyaniline as conductive polymers have unique advantages, including a large amount of nitrogen-containing functional groups, low cost, simple preparation, and good environmental stability.[7,8] The copolymerization of pyrrole and aniline on the short-channel SBA-15 can greatly improve the adsorption effect of the short-channel SBA-15. Especially nitrogen-containing functional groups produced after copolymerization have unique advantages for heavy metal pollution (especially mercury[9] and chromium[10] contamination) in water.

Received: August 8, 2021
Accepted: September 9, 2021
Published: September 23, 2021

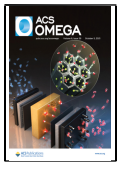

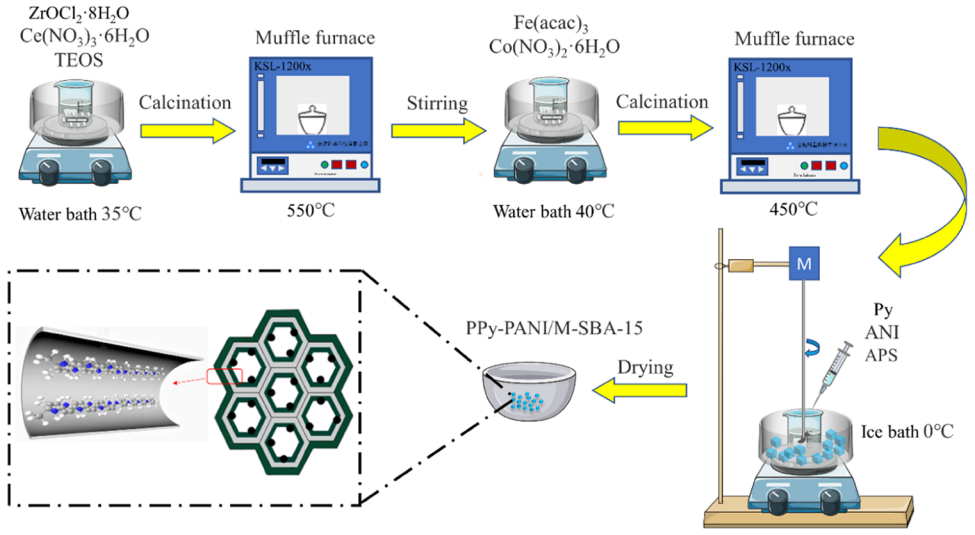

Figure 1. Preparation flow chart of PPy-PANI/M-SBA-15.

In addition, regeneration performance can be resolved by improving the solid−liquid separation efficiency of SBA-15. The magnetic material of cobalt ferrite ($CoFe_2O_4$) is introduced into the short-channel SBA-15 to prepare an SBA-15 magnetism composite, thereby making recycling easy to implement.[11] In this study, the magnetic short-channel SBA-15 mesoporous molecular sieve avoids the disordered growth and forms a spherical shape when pyrrole and aniline are copolymerized by virtue of their platelet state. Both the possibility of agglomeration and the disadvantage of the low density of polymer functional groups are also alleviated.

This paper aims to focus on the modification and application of short-channel SBA-15 mesoporous molecular sieves by copolymers of polypyrrole (PPy) and polyaniline (PANI) to form magnetic composites with nitrogen-containing functional groups to remove mercury ions from aqueous solutions. The synthesized PPy-PANI/M-SBA-15 composites were physically and chemically characterized using various instruments. Meanwhile, by considering the effects of pH, mercury concentration, adsorbent dosage, temperature, and contact time, the optimal adsorption conditions of PPy-PANI/M-SBA-15 composites for mercury ions were evaluated by the response surface method (RSM) and central composite design (CCD) method, and a possibility adsorption mechanism was also proposed.

2. EXPERIMENTAL METHODS

2.1. Chemicals and Materials. Triblock copolymer $EO_{20}PO_{70}EO_{20}$ (P123, Aldrich, M_a = 5800), tetraethyl orthosilicate (TEOS), zirconium oxychloride octahydrate ($ZrOCl_2·8H_2O$), and cerium(III) nitrate hexahydrate ($Ce(NO_3)_3·6H_2O$) were obtained from Macklin Reagent Co., Ltd. (China). Cobaltous nitrate hexahydrate ($Co(NO_3)·2H_2O$), pyrrole monomer (Py, 98%), aniline monomer (Ani, 98%), ammonium persulphate ($(NH_4)_2S_2O_8$), hydrochloric acid (HCl), and sodium hydroxide (NaOH) were provided by Sinopharm Chemical Reagent Co., Ltd. (China). All reagents and drugs used were of analytical grade.

2.2. Synthesis of Short-Channel SBA-15 Mesoporous Silica (SBA-15). The preparation of short-hole SBA-15 was described in our previous work.[6] The required material was added to a beaker in a ratio of P123/TEOS/$ZrOCl_2·8H_2O$/$Ce(NO_3)·H_2O$/H_2O = 0.01:1:0.05:0.05:170 to continue the reaction at 308 K for 20 h. After maintaining at 373 K for 24 h, the product was filtered, washed, and dried. Ultimately, calcination was carried out for 6 h at 823 K to remove the templating agent.

2.3. Synthesis of Magnetic Short-Channel SBA-15 (M-SBA-15). $Fe(caca)_3$ and cobalt nitrate were added into 10 mL of pure aqueous solution in a molar ratio of 2:1, and then the solution (pH = 5) was stirred for 30 min at 318 K. Then, 0.25 g of SBA-15 was added and continued to be stirred for 12 h. After centrifugation, the product was dried in an oven at 333 K overnight, followed by calcination at 723 K for 2 h, and the obtained material was named M-SBA-15.

2.4. Synthesis of Polypyrrole/Polyaniline Copolymer-Coated Magnetic Short-Channel SBA-15 (PPy-PANI/M-SBA-15). Briefly, 0.05 mL of Py and Ani monomers were added to a glass jar with 10 min of ultrasound treatment. Afterward, 0.1 g of magnetic M-SBA-15 was added and sonicated for 1 h. The above mixture was transferred to a beaker using 33 mL of 1 M HCl solution, and then mechanically stirred for 1 h in an ice bath. About 0.23 g of $(NH_4)_2S_2O_8$ was dissolved in 1 mL of aqueous solution, and then added dropwise to the mixture with stirring for 6 h.

After that, the product was washed with distilled water under external magnetic field conditions until the supernatant was colorless, and finally dried in a vacuum oven at 333 K for 8 h. The prepared magnetic SBA-15 coated with the pyrrole and aniline copolymer is named PPy-PANI/M-SBA-15. A related schematic diagram of the preparation process and structure can be referred to in Figure 1.

2.5. Batch Experiments. The batch adsorption experiment was carried out at a set temperature and time by placing a stoppered Erlenmeyer flask containing 100 mL of the desired concentration of mercury ion solution and adsorbent in a constant temperature oscillator. The constant temperature oscillator was used at a speed of 150 rpm throughout the test. After adsorption, the adsorbent was separated by an external magnetic field, and the residual mercury ion concentration was measured with a cold atomic absorption spectrophotometer. In this way, the effects of pH, adsorbent dosage, contact time, temperature, and ion concentration on adsorption were all investigated. All experiments were performed three times, and

https://doi.org/10.1021/acsomega.1c04249
ACS Omega 2021, 6, 25791−25806

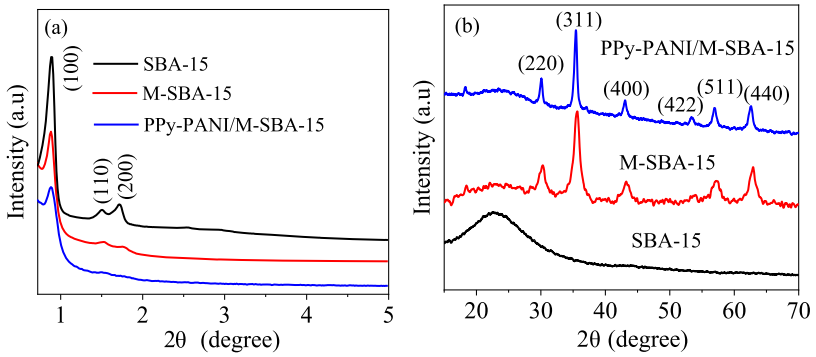

Figure 2. XRD spectra of SBA-15, M-SBA-15, and PPy-PANI/M-SBA-15: small-angle XRD spectrum (a) and wide-angle XRD spectrum (b).

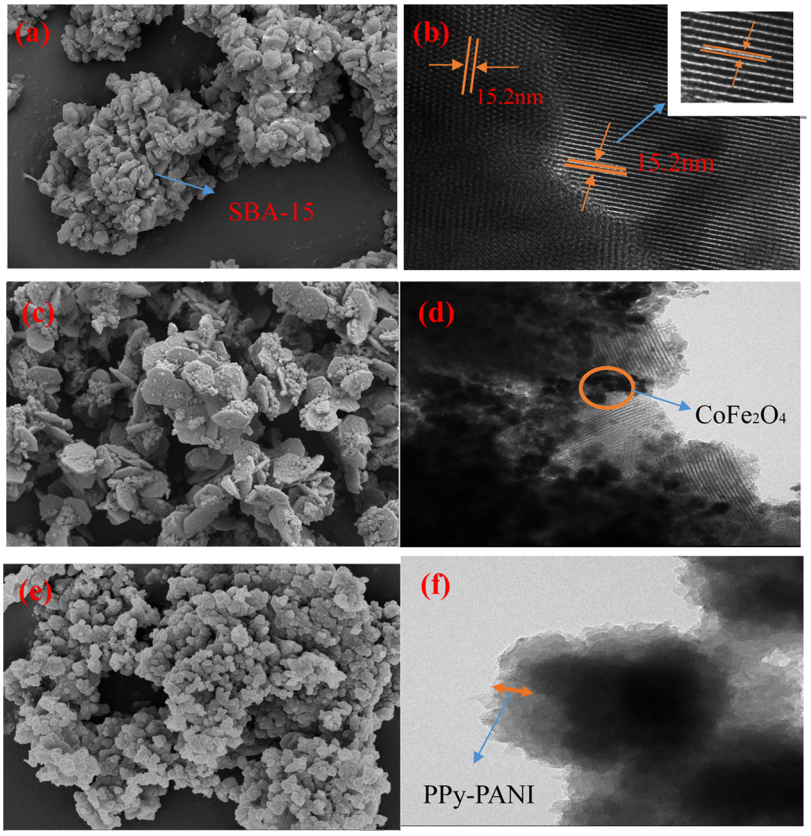

Figure 3. SEM and transmission electron microscopy (TEM) images of SBA-15 (a, b), M-SBA-15 (c, d), and PPy-PANI/M-SBA-15 (e, f).

the average value of the experimental results was used as the final result.

According to eq 1, the adsorption capacity at equilibrium can be calculated using

$$q_e = \frac{(C_0 - C_e)}{W} \times V \quad (1)$$

wherein C_0 and C_e are the concentrations of Hg(II) initial and equilibrium adsorption (mg/L), respectively, V (L) is the solution volume, and W (g) is the adsorbent dosage.

2.6. Effect of pH. The adsorbent was added to a stoppered conical flask containing 100 mL of 30 mg/L mercury solution. The solution pH value was measured with a pH meter. The effect of the solution pH on the adsorption was investigated by dropwise addition of HCl and NaOH so that the solution pH was between 2 and 8. The solution was oscillated at 298 K for 6 h to achieve adsorption equilibrium.

2.7. Effect of Dosage. Different dosages of the adsorbent (0.02−0.12 g/L) were added to test its effect on adsorption. The concentration, volume, and pH of the solution are 30 mg/L, 100 mL, and 7, respectively. The solution was oscillated at 298 K for 6 h to reach adsorption equilibrium.

2.8. Kinetic Experiments. About 0.015 g of the adsorbents was added into a beaker containing 300 mL of 30 mg/L mercury solution, and then was stirred at a rate of 150 rpm. A quantity of 2 mL of the sample was taken after different time intervals (0−420 min), followed by the detection of the instantaneous concentration.

2.9. Isothermal and Thermodynamic Experiments. The effect of temperature on adsorption was obtained under the following conditions: concentration of 30 mg/L, dosage of 0.05 g/L, pH = 7, and a temperature of 298−308 K. The final adsorption dosage was obtained by calculating the residual

https://doi.org/10.1021/acsomega.1c04249
ACS Omega 2021, 6, 25791−25806

concentration and initial concentration of mercury ions after shaking for 6 h.

3. RESULTS AND DISCUSSION

3.1. Characterizations. The physical and chemical characterization instruments can be found in our previous reports. Figure 2a shows small-angle X-ray diffraction (XRD) spectra of SBA-15, magnetic M-SBA-15, and polypyrrole/polyaniline copolymer-modified PPy-PANI/M-SBA-15. It can be clearly seen that the M-SBA-15 sample has obvious (100), (110), and (200) diffraction peaks, attributed to the two-dimensional hexagonal *P6mm* symmetry. It is shown that M-SBA-15 retains the presence of highly ordered mesoporosity.[12]

The (110) and (200) diffraction peaks of the M-SBA-15-modified pyrrole and aniline copolymers to become less noticeable, which may be caused by the formation of the polymer, causing some fine pores to be clogged.[13] The diffraction peaks of M-SBA-15 and PPy-PANI/M-SBA-15 are wider and less intense than that of pure SBA-15, indicating that $CoFe_2O_4$ and the copolymer enter the mesopores of SBA-15.[6,14]

Figure 2b shows the wide-angle XRD spectrum of the three materials. It can be seen that there is a broad peak at 23° in the SBA-15 spectrum, revealing the amorphous nature of silica.[15] Meanwhile, after $Fe(acac)_3$ and cobalt nitrate hexahydrate were impregnated into the pores of SBA-15 and calcined at a high temperature, the diffraction peak attributed to the $CoFe_2O_4$ nanoparticles appears in the XRD spectrum of M-SBA-15.[16] There is no new diffraction peak in the XRD pattern of M-SBA-15 modified by the pyrrole and aniline copolymer. In addition, the peak values of PPy-PANI/M-SBA-15 appear to be the same as those of M-SBA-15. The result indicates that the M-SBA-15 material has no change in the crystal form after modification.

Table 1. Data for SBA-15, M-SBA-15, and PPy-PANI/M-SBA-15

samples	BET values (m^2/g)	total pore volumes (cm^3/g)	pore diameters (nm)
$CoFe_2O_4$	48.36	0.38	17.08
SBA-15	148.74	0.67	15.82
M-SBA-15	108.36	0.32	6.55
PPy-PANI/M-SBA-15	12.30	0.03	3.31

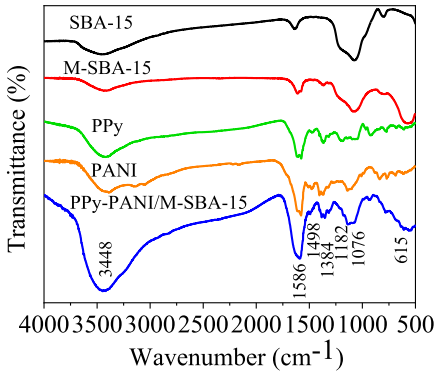

Figure 4. FT-IR spectra of SBA-15, M-SBA-15, PPy, PANI, and PPy-PANI/M-SBA-15.

The morphologies of SBA-15, M-SBA-15, and PPy-PANI/M-SBA-15 were investigated by scanning electron microscopy (SEM). As shown in Figure 3a, SBA-15 has a platelet-like morphology and exhibits a uniform size of about 12 nm. The PPy-PANI/M-SBA-15 nanoparticle has a similar morphology as the original SBA-15 (Figure 3c) and becomes irregular in appearance and does not have the original hexagonal plate shape. This may be due to the fact that pyrrole and aniline are also copolymerized outside M-SBA-15.

TEM analysis was performed to directly observe the coating of $CoFe_2O_4$, pyrrole, and aniline copolymers onto SBA-15. As shown in Figure 3b, SBA-15 has a two-dimensional hexagonal pore structure unique to mesoporous molecular sieves.[17] This highly ordered mesoporous material supports the possibility of incorporating $CoFe_2O_4$ nanoparticles. As expected, $CoFe_2O_4$ was incorporated into the pores of SBA-15, which can be observed in Figure 3d, and the material still retains the hexagonal pore structure, indicating that the entry of $CoFe_2O_4$ nanoparticles does not change its microstructure.[18]

According to Figure 3e–f, the polymerization of pyrrole and aniline occurs in the pores of M-SBA-15 and outside M-SBA-15, which is also consistent with the morphological characterization of SEM. The phenomenon can further support the conclusions given in Table 1. The specific surface area of PPy-PANI/M-SBA-15 is smaller than those of M-SBA-15 and SBA-15.

The EDS spectrum and EDX elemental mapping of PPy-PANI/M-SBA-15 are shown in Figure S1a–g (Supporting Information), which further proves that PPy-PANI/M-SBA-15 is successfully synthesized. The constituent elements only contain C, N, O, Fe, Co, and Si elements, which was consistent with the subsequent X-ray photoelectron spectroscopy (XPS) results, and these elements are evenly distributed on PPy-PANI/M-SBA-15.

To demonstrate the successful loading of the copolymer of pyrrole and aniline on M-SBA-15, Fourier transform infrared (FT-IR) analysis was performed on PPy, PANI, and PPy-PANI/M-SBA-15, and the results are shown in Figure 4. It can be seen that the peak at 3448 cm^{-1} represents the stretching vibrations of −OH in water molecules, and the peaks at 802 and 1088 cm^{-1} represent SiO_2[19] and a new peak representing the Fe−O and the Co−O bonds appears at 615 cm^{-1}, demonstrating the successful synthesis of $CoFe_2O_4$ nanoparticles.[20]

The FT-IR spectrum of polypyrrole shows the characteristic peak of PPy at 1576 cm^{-1}, which is the stretching vibration of C═C in the pyrrole ring.[21] The vibrational peaks at 928, 1040, 1193, and 1364 cm^{-1}, respectively, represent the bending vibrations of the C−H bond deformed inside and outside the plane, the −N bond in the plane vibration, and the tensile vibrations of the C−N bond in the pyrrole ring.[22,23]

The FT-IR spectrum of polyaniline shows a vibration peak of PANI at 1578 cm^{-1}, which is the C═C stretching vibrations of the quinone.[24] The peaks at 771, 1103, 1319, and 1478 cm^{-1} of the spectrum are attributable to the C−H bond in the PANI ring, the tensile vibrations of the C═N bond and the CN bond, and the stretching vibrations of the benzene ring, respectively.[25,26]

The characteristic peaks representing PPy and PANI can be found in the spectrum of PPy-PANI/M-SBA-15. Some peaks representing the C−C bond and the C−N bond can be observed in the spectrum after the copolymerization of pyrrole and aniline, which transfers to high wavenumbers of 930, 1076,

https://doi.org/10.1021/acsomega.1c04249
ACS Omega 2021, 6, 25791−25806

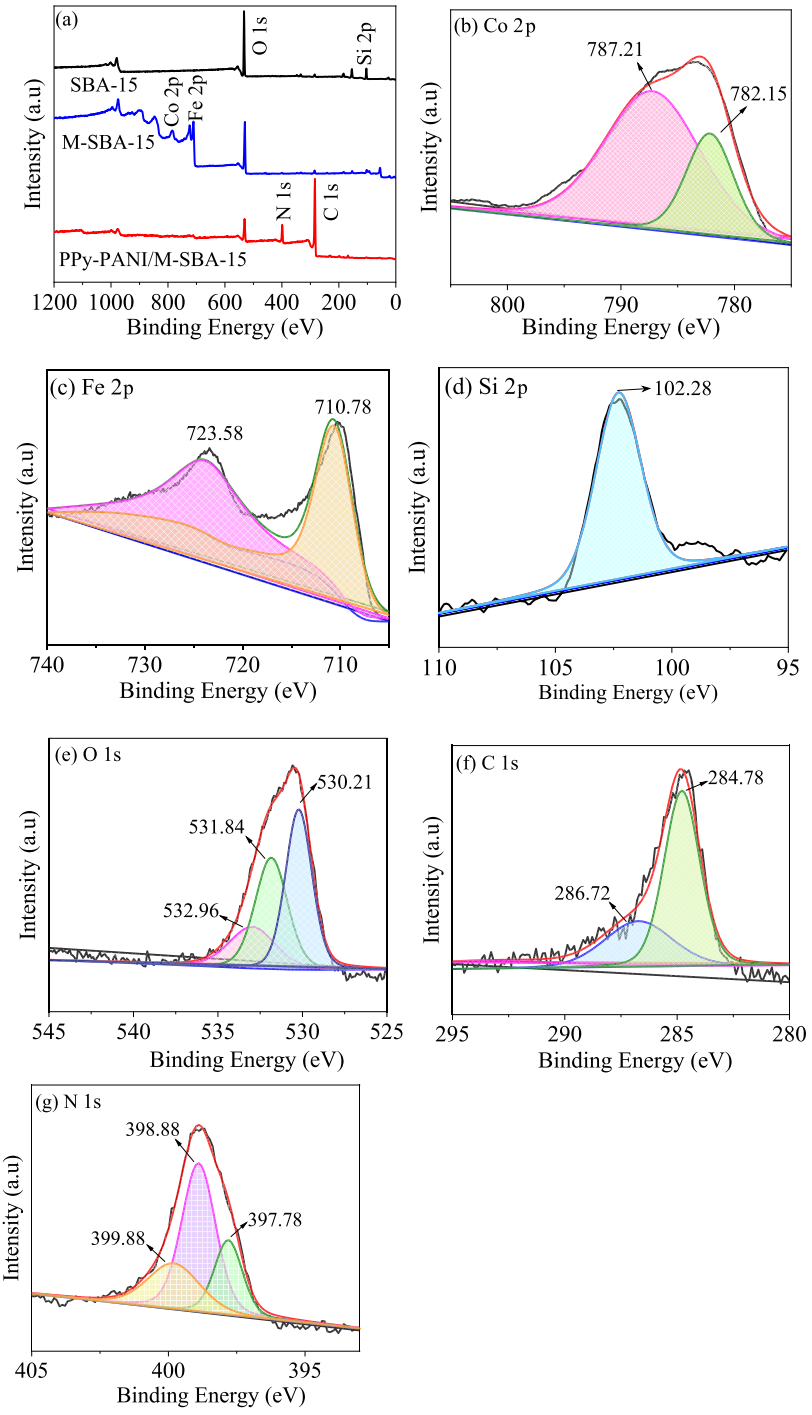

Figure 5. XPS spectra of SBA-15, M-SBA-15, and PPy-PANI/M-SBA-15 composites in the range of 0−1200 cm^{-1} (a), core energy spectra of each element before adsorption: Co 2p (b), Fe 2p (c), Si 2p (d), O 1s (e), C 1s (f), and N 1s (g).

and 1384 cm^{-1}. At 1103 cm^{-1}, the characteristic peak representing the C═C bond in PANI is also converted to 1182 cm^{-1}. Simultaneously, the peaks representing the C═C bonds of the pyrrole ring and the benzene ring in PANI have shifted to high wavenumbers of 1586 and 1498 cm^{-1}.

Compared with pure PPy and PNAI, the characteristic peaks of PPy-PANI/M-SBA-15 slightly shift to high wavenumbers, which may be due to the strong interaction after the copolymerization of PPy and PANI and M-SBA-15. It has been reported that changes in the peak position may be caused by oscillations in the polymer backbone due to resonance coupling.[12,15] However, on the final prepared adsorbent, new characteristic peaks representing PPy and PANI can be detected, indicating that the copolymer of pyrrole and aniline was successfully loaded onto M-SBA-15, and the adsorbent PPy-PANI/M-SBA-15 was successfully prepared.

Figure 5a−g shows an XPS measurement spectrum of SBA-15, M-SBA-15, and PPy-PANI/M-SBA-15 composites. The full range of the XPS spectrum (Figure 5a) shows the presence of Co 2p (785.08 eV), Fe 2p (711.08 eV), O 1s (533.08 eV), Si 2p (102.28 eV), C 1s (284.08 eV), and N 1s (399.08 eV). It can be seen from Figure 5b,c that Co 2p and Fe 2p appear in

https://doi.org/10.1021/acsomega.1c04249
ACS Omega 2021, 6, 25791−25806

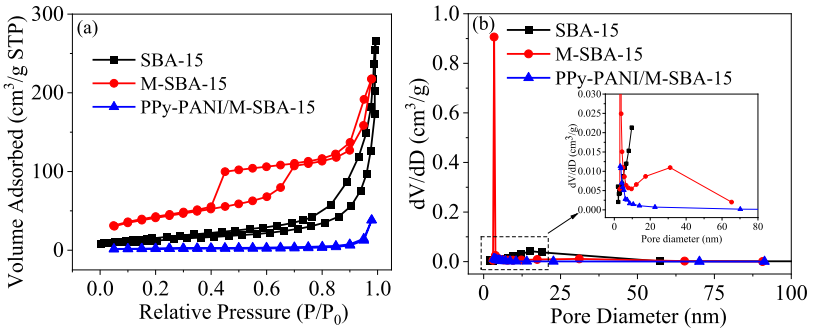

Figure 6. N_2 adsorption−desorption isotherms (a) and pore diameter of materials (b).

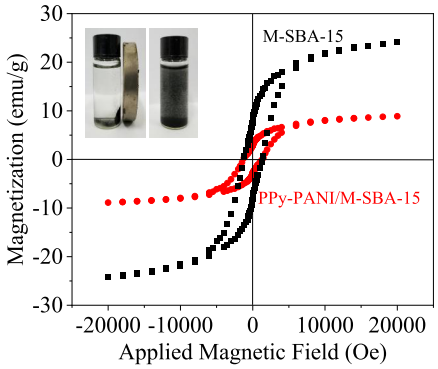

Figure 7. Magnetization curve measured for M-SBA-15 and PPy-PANI/M-SBA-15 (inserted picture: the separation of PPy-PANI/M-SBA-15 by an external magnet).

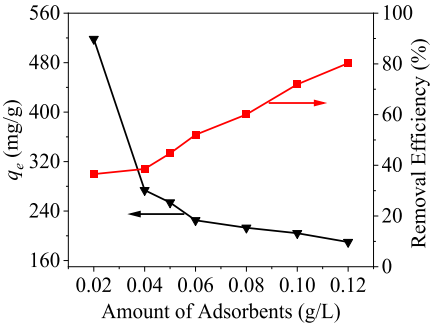

Figure 9. Influence of the amount of adsorbents on Hg(II) adsorption. (pH = 7, temperature = 298 K, [Hg(II)] = 30 mg/L, contact time = 6 h).

the M-SBA-15 spectrum, indicating that $CoFe_2O_4$ was successfully loaded in the material, making SBA-15 magnetic.

The PPy-PANI/M-SBA-15 composite has two peaks of C 1s and N 1s, which is caused by the carbon and nitrogen elements of the pyrrole and aniline copolymers. The successful introduction of pyrrole and aniline copolymers during the process of synthesis is consistent with the results of FT-IR analysis.

The binding energies of the N 1s core energy spectrum of the PPy-PANI/M-SBA-15 composite shown in Figure 5g at 397.78, 398.88, and 399.88 eV correspond to the quinone imine (=N−), benzylamine (−NH−), and electronically doped imine ($-NH^+-$), respectively. These are the characteristics of PPy and PANI, and their existence also proves that the copolymer of polypyrrole/polyaniline was successfully compounded onto M-SBA-15.[27]

The nitrogen adsorption−desorption isotherm and pore size distribution maps for all samples are shown in Figure 6. The isotherms of the corresponding samples show a type IV isotherm and an H1 type adsorption hysteresis loop at relatively high pressures. A typical feature of mesoporous materials is that they have capillary condensation and a large pore size and a narrow pore size distribution. The relative pressure of P/P_0 of SBA-15 is <0.7, as expected for mesoporous materials.[28]

Table 1 lists the Brunauer−Emmett−Teller (BET) specific surface area, pore volume, and pore size data for the corresponding samples. The results show that the surface area, pore volume, and pore size of the SBA-15 doped with $CoFe_2O_4$ nanoparticles are reduced compared with SBA-15, which may be due to the formation of $CoFe_2O_4$ nanoparticles in the pores and outer faces. The result is also consistent with the data shown in Figure 6a,b, where the apparent relative

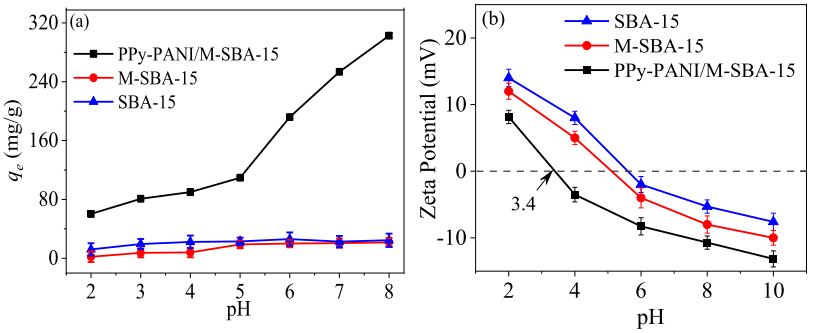

Figure 8. Influence of pH on Hg(II) adsorption (dosage = 0.05 g/L, temperature = 298 K, [Hg(II)] = 30 mg/L, contact time = 6 h) (a) and ζ potential curve diagram of SBA-15, M-SBA-15, and PPy-PANI/M-SBA-15 (b).

https://doi.org/10.1021/acsomega.1c04249
ACS Omega 2021, 6, 25791−25806

Table 2. CCD Matrix and Running Results Obtained by PPy-PANI/M-SBA-15

		variables				
std.	run	pH (A)	T (B)	C_0 (C)	dosage (D)	response (q_e)
3	1	5	40	20	0.04	213.4
25	2	6	35	30	0.05	320
20	3	6	45	30	0.05	308
15	4	5	40	40	0.06	215.6
29	5	6	35	30	0.05	321
7	6	5	40	40	0.04	213.4
13	7	5	30	40	0.06	239.8
14	8	7	30	40	0.06	320
9	9	5	30	20	0.06	228.8
12	10	7	40	20	0.06	294.8
5	11	5	30	40	0.04	197.5
8	12	7	40	40	0.04	367
18	13	8	35	30	0.05	325
19	14	6	25	30	0.05	260
10	15	7	30	20	0.06	258
26	16	6	35	30	0.05	322
28	17	6	35	30	0.05	322
24	18	6	35	30	0.07	276.1
1	19	5	30	20	0.04	191
2	20	7	30	20	0.04	247
16	21	7	40	40	0.06	351
27	22	6	35	30	0.05	323
6	23	7	30	40	0.04	308
4	24	7	40	20	0.04	315
17	25	4	35	30	0.05	142
21	26	6	35	10	0.05	231
30	27	6	35	30	0.05	323
11	28	5	40	20	0.06	223.3
22	29	6	35	50	0.05	287.1
23	30	6	35	30	0.03	254.1

pressure of M-SBA-15 shifts to a smaller 0.4 direction than SBA-15, indicating a decrease in pore size.[29]

The surface area, pore volume, and pore size of PPy-PANI/M-SBA-15 become small, probably owing to the large number of chain pyrrole and aniline copolymers during the process of continuous polymerization and filling of the copolymers in the channels and surfaces of the material. On the one hand, the successful polymerization of pyrrole and aniline on M-SBA-15 was demonstrated; on the other hand, the result also indirectly reflects that the specific surface area of the material does not play a major role. Related research phenomena and conclusions are also reflected in some literature studies.[30,31]

Figure 7 shows the hysteresis loops of M-SBA-15 and PPy-PANI/M-SBA-15 at 298 K. The saturation magnetization of M-SBA-15 is 23.11 emu/g, and the saturation magnetization of the adsorbent sample after modification is reduced to 8.21 emu/g, which is approximately a straight line.

The saturation magnetic strength in the material is mainly contributed by $CoFe_2O_4$ nanoparticles. The lowered saturation magnetic intensity of PPy-PANI/M-SBA-15 resulted from the decrease of the relative content of the magnetic components due to the addition of pyrrole and aniline. It can be seen from the inserted picture that PPy-PANI/M-SBA-15 is uniformly diffused in water and can be rapidly adsorbed in 1 min under the action of an external magnetic field, which proves that PPy-PANI/M-SBA-15 has better magnetic properties.

3.2. Adsorption Performance Test. *3.2.1. Effect of pH.* As one of the factors for controlling the amount of metal ions adsorbed by the adsorbent, solution pH plays an important role during the process of entire adsorption. The adsorption capacity was measured by adjusting the pH in the range of 2−8, while the others include temperature, contact time, sorbent dosage, and metal ion concentration. The effect of pH change on Hg(II) removal is shown in Figure 8a.

As we can see from Figure 8a, the prepared short-channel SBA-15 has a relatively low adsorption capacity for Hg(II). In addition, after the magnetic particles of $CoFe_2O_4$ are supported on SBA-15 to form M-SBA-15, its adsorption capacity for Hg(II) is lower than that of pure short-channel SBA-15, which is attributed to a low surface area of M-SBA-15 caused by $CoFe_2O_4$ loading.[32] The result indicates that the magnetic particles of $CoFe_2O_4$ have a negligible Hg(II) capturing capability, compared with the PPy-PANI/M-SBA-15.

By contrast, as for the modified compound PPy-PANI/M-SBA-15, the adsorption capacity for Hg(II) at pH = 2 is 60.3 mg/g. With the increase of pH, when the pH reaches 8, the adsorption capacity of PPy-PANI/M-SBA-15 reaches 302.7 mg/g. However, when pH = 8, mercury ions form hydroxides such that the solubility decreases, resulting in an increase in the removal rate. Therefore, in the experiment, pH = 7 was selected as the optimum value, and the adsorption amount under the pH also reaches a high value of 253.8 mg/g, which is greatly improved compared with those of pure SBA-15 (45.9 mg/g) and M-SBA-15 (39.2 mg/g) under the same conditions.

At low pH values, mercury ions are repelled due to protonation of the adsorbent surface. Simultaneously, a high concentration of H^+ in the aqueous solution at a low pH makes it compete with the mercury ions for the active sites on the surface of the adsorbent, resulting in a low removal rate.[33] As the pH increases, the concentration of H^+ ions decrease, and the competition between the mercury ions and H^+ ions reduce, resulting in an increase in the adsorption capacity.

As shown in Figure 8b, the surface potentials of SBA-15, M-SBA-15, and PPy-PANI/M-SBA-15 were measured with a ζ potentiometer, and it can be seen that the isoelectric point (pH_{zpc}) of PPy-PANI/M-SBA-15 is 3.4. Therefore, when the pH $\geq$ 3.4, PPy-PANI/M-SBA-15 is negatively charged. The main reason is that PPy and PANI contain a lot of amino groups after SBA-15 is modified by PPy and PANI.[34] The ζ potential of PPy-PANI/M-SBA-15 is −9.5 mV at pH = 7, which is lower than that of SBA-15 (−3.6 mV). The results

Table 3. Summary Statistics of the Four Models

mode	std. dev.	R^2	R_{adj}^2	R_{pre}^2	discrepancy	
linear	33.10	0.6878	0.6378	0.5916	35 836.87	
2FI	32.74	0.7679	0.6458	0.6144	33 835.21	
quadratic	1.99	0.9993	0.9987	0.9964	313.98	suggested
cubic	1.99	0.9997	0.9987	0.9657	3011.28	

https://doi.org/10.1021/acsomega.1c04249
ACS Omega 2021, 6, 25791−25806

Table 4. Results of ANOVA of the Quadratic Model

terms	sum of square	df	mean square	*F*-values	*p*-values	
model	87 685.45	14	6263.25	1575.40	<0.0001	significant
A (pH)	50 784.00	1	50 784.00	12 773.71	<0.0001	
B (T)	3735.01	1	3735.01	939.47	<0.0001	
C (C_0)	5197.93	1	5197.93	1307.44	<0.0001	
D (dosage)	630.38	1	630.38	158.56	<0.0001	
AB	2166.90	1	2166.90	545.04	<0.0001	
AC	3063.62	1	3063.62	770.59	<0.0001	
AD	694.32	1	694.32	174.64	<0.0001	
BC	100.00	1	100.00	25.15	0.0002	
BD	1011.24	1	1011.24	254.36	<0.0001	
CD	0.2500	1	0.2500	0.0629	0.8054	
A^2	13 162.53	1	13 162.53	3310.77	<0.0001	
B^2	2362.74	1	2362.74	594.30	<0.0001	
C^2	6605.67	1	6605.67	1661.52	<0.0001	
D^2	5380.80	1	5380.80	1353.43	<0.0001	
residual	59.63	15	3.98			
lack of fit	52.80	10	5.28	3.86	0.0744	not significant
pure error	6.83	5	1.37			
cor total	87 745.09	29				

show that the surface potential of PPy-PANI/M-SBA-15 is negative under higher pH conditions, so its surface is negatively charged, which can greatly enhance the electrostatic attraction and the adsorption capacity of Hg(II).

3.2.2. Effect of Dosage. The effect of adsorbent dosage on the adsorption of mercury ions obtained in Figure 9 shows that PPy-PANI/M-SBA-15 is an effective adsorbent for removing mercury ions from aqueous solution. It can be seen from Figure 9 that as the adsorption dose increases, the mercury ion removal rate also increases, but the adsorption capacity decreases. This is because the increase in the amount of the adsorbent increases the available amount of active sites, and the probability of adsorption of mercury ions in the solution also increases.[35]

However, due to the increase in the number of active adsorption sites, the effective utilization rate is reduced. When the amount of PPy-PANI/M-SBA-15 added is 0.05 g/L, the adsorption capacity and removal efficiency can reach 253.8 mg/g and 44.7%, respectively. Therefore, considering the balance of adsorption capacity and removal efficiency, the addition amount of PPy-PANI/M-SBA-15 is set as 0.05 g/L.

3.2.3. Optimization of Experimental Conditions by RSM. Based on the above preliminary experiments, the appropriate range for the studied factors in the RSM has been well determined. Moreover, to further study the optimal adsorption conditions for the maximum adsorption capacity, Design-Expert 11.0 software was used to get a central composite design (CCD) matrix to design batch experiments.[36]

A total of 30 running experiments involve 4 independent variables, including 5 code value points (−2, −1, 0, + 1 +2), 18 design points on 6 axes, and 6 duplicates at the center point.[34,37] The pH range is 4−8, the adsorption temperature is 25−45°C, the C_0 is 10−50 mg/L, and the dosage is 0.03−0.07 g/L. The adsorption quantity q_e is the response variable (Response), and the experimental results are shown in Table 2.

ANOVA is employed to investigate the significance of the model and the relationship between each variable and the response variable.[38] The relationship between responses and variables and the correlation among variables are expressed in the quadratic regression model in the coded form [eq 2] and in the uncoded form [eq 3].

$$q_e = 321.83 + 46A + 12.47B + 14.72C + 5.13D + 11.64AB + 13.84AC - 6.59AD - 2.5BC - 7.95BD + 0.125CD - 21.91A^2 - 9.28B^2 - 15.52C^2 - 14.01D^2 \quad (2)$$

$$q_e = -1633.15 + 218.84 \times \mathrm{pH} + 23.97 \times T + 4.17 \times C_0 + 23998.75 \times \mathrm{dosage} + 2.33 \times \mathrm{pH} \times T + 1.38 \times \mathrm{pH} \times C_0 - 658.75 \times \mathrm{pH} \times \mathrm{dosage} - 0.05 \times T \times C_0 - 159 \times T \times \mathrm{dosage} + 1.25 \times C_0 \times \mathrm{dosage} - 21.91 \times \mathrm{pH}^2 - 0.37 \times TT^2 - 0.16 \times {C_0}^2 - 1.4 \times 10^5 \times \mathrm{dosage}^2 \quad (3)$$

As shown in Tables 2 and 3, four different models, namely, linear, two factor interaction (2FI), quadratic, and cubic models, were used to fit the experimental results. Compared with other models, the quadratic model (quadratic) has a high coefficient of certainty (R^2 = 0.9980). The adjusted coefficient (${R_{adj}}^2$ = 0.9962) and the predicted coefficient of certainty (${R_{pre}}^2$ = 0.9886) are also the highest, which indicates that the quadratic model is the most suitable model.

The pH (A), temperature T (B), initial concentration of mercury solution C_0 (C), and the amount of adsorbents (D) and their interaction can also be obtained from the variance analysis (Table 4) of the quadratic model. In addition, the terms of A, B, C, D, AB, AC, AD, BD, A^2, B^2, C^2, and D^2 have significant influence on adsorption abilities. Among them, the synergistic factor effects are as follows: pH (A) > C_0 (C) > T (B) > dosing amount (D), which is judged by their corresponding F-values. The F-value of the quadratic model is 538.64 and p-value is less than 0.0001, which indicate that the adsorption quantity q_e of PPy-PANI/M-SBA-15 is a

https://doi.org/10.1021/acsomega.1c04249
ACS Omega 2021, 6, 25791−25806

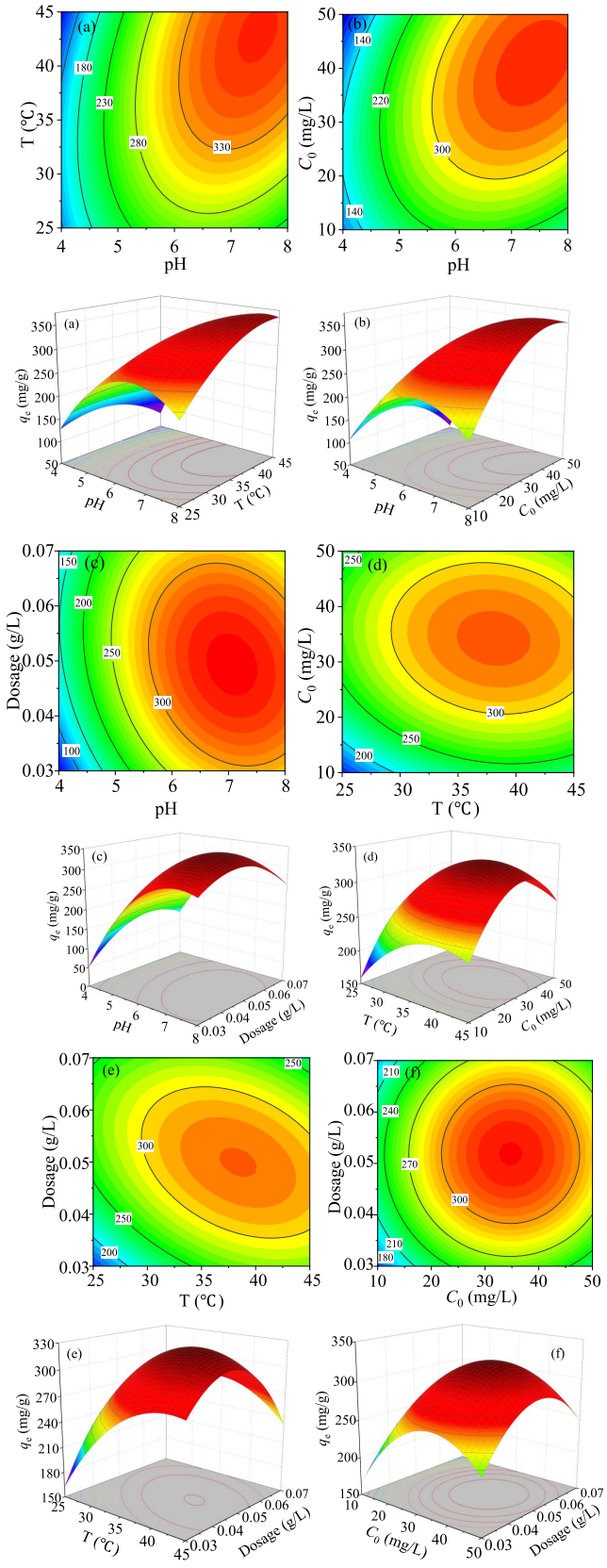

Figure 10. 3D relationship between variables and q_e: pH and temperature (a); pH and C_0 (b); pH and dosage (c); temperature and C_0 (d); temperature and dosage (e); and C_0 and dosage (f).

significant influence factor. Based on the above analysis, it is proved that the quadratic model is the most suitable model.[37]

Figure 10a is a three-dimensional (3D) ascending map between the pH (A) and temperature (B). The adsorption conditions are that C_0 is 30 mg/L, the dosage is 0.05 g/L, and the adsorption time is 24 h. When the pH range is 7.2−7.8 and the temperature range is 40−45 °C, the adsorbent has the largest adsorption capacity for mercury ions, and q_e is between 300 and 350 mg/g. The minimum adsorption capacity is under the conditions of pH < 6 and low temperature. This is because as the pH increases, when the pH is higher than pH_{zpc}, the surface charge of PPy-PANI/M-SBA-15 is negative, which can provide more equipotential points to adsorb mercury ions. Table 4 shows that AB is significant (*F*-value = 545.04, *p*-value < 0.0001) on the adsorption process.

Figure 10b is the 3D ascending map between pH (A) and C_0 (C) at the temperature of 35 °C and dosage of 0.05 g/L. When the pH range is 6.8−7.8 and C_0 is 35−45 mg/L, the adsorbent has the largest adsorption capacity for mercury ions and the q_e is between 300 and 350 mg/g. It is because only when mercury ions reach a certain concentration (35−45 mg/L), the adsorption capacity of the material can reach saturation under certain conditions (T = 35 °C, dosage = 0.05 g/L). In addition, the *F*-value (770.59) and the *p*-value (<0.0001) in Table 4 indicate that AC has a significant effect on the adsorption process.

Figure 10c is the ascending map between pH (A) and the dosage (D). The adsorption conditions are that the solution temperature is 35 °C, C_0 is 30 mg/L, and the adsorption time is 24 h. When the pH concentration is 6.8−7.5 and the dosage is 0.045−0.055 g/L, the adsorbent has the largest adsorption capacity for mercury ions, and the q_e is between 300 and 350 mg/g. Meanwhile, it can be seen that with the increase of pH and dosage, the adsorption performance continues to increase. It can be seen from Table 4 that AD is significant (*F*-value = 174.64, *p*-value < 0.0001).

Figure 10d shows the interaction of temperature (B) and C_0 (C) on the adsorption capacity. The experiment was carried out under the conditions of pH = 6 and dosage = 0.05 g/L. It can be seen that the maximum adsorption capacity is within the range of the temperature of 35−42 °C and the C_0 of 30−38 mg/L. The *F*-value (254.36) and *p*-value (0.0002) of BC in Table 4 prove that the influence of BC on the adsorption effect is significant.

Figure 10e shows the interaction of temperature (B) and dosage (D) on q_e at pH = 6 and C_0 = 30 mg/L. When the temperature is between 36 and 40 °C and the dosage is between 0.045 and 0.052 g/L, the adsorption capacity of the adsorbent for Hg(II) reaches the maximum (300−330 mg/g). Figure 10f shows the combined impact of C_0 (C) and the dosage (D) on the adsorption capacity q_e at pH = 6 and T = 35 °C. The maximum adsorption capacity (300−350 mg/g) is within the range of C_0 = 30−40 mg/L and the dosage of 0.045−0.055 g/L. In Table 4, we can see that the term of BD (*F*-value = 254.36, *p*-value < 0.0001) is significant, but the term of CD (*F*-value = 0.0629, *p*-value = 0.8054) is not a significant factor.

In other words, the combined effect of all operational parameters analyzed by the RSM method indicates that the maximum adsorption capacity of 346.2 mg/g was acquired under the optimal conditions of pH of 6.7, temperature of 310 K, C_0 of 29.5 mg/L, and dosage of 0.044 g/L.

3.3. Kinetic Experiments. To study the equilibrium time required to achieve the maximum removal rate and to understand the kinetics of the adsorption process, this

https://doi.org/10.1021/acsomega.1c04249
ACS Omega 2021, 6, 25791−25806

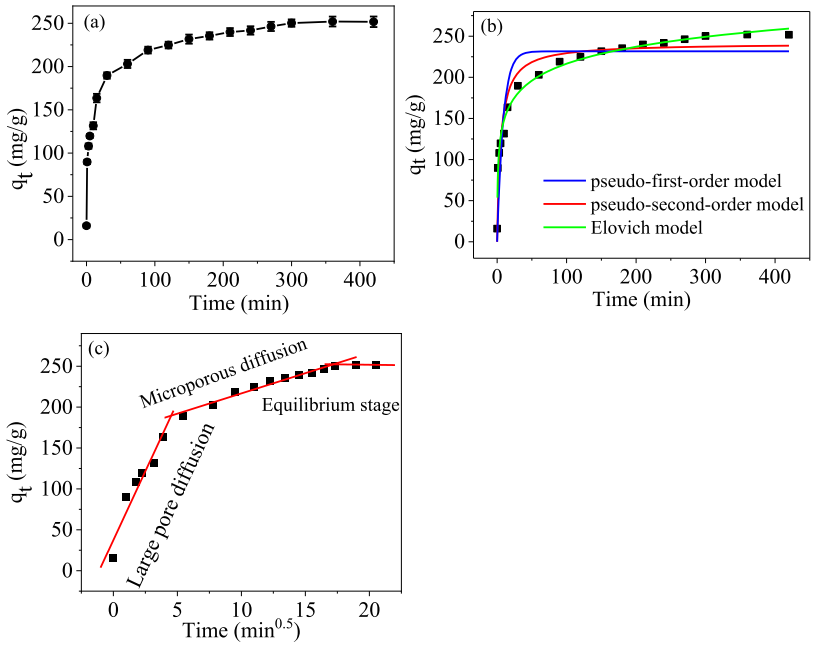

Figure 11. Adsorption capacity vs contact time (a), kinetic fitting results (b), and particle diffusion model (c).

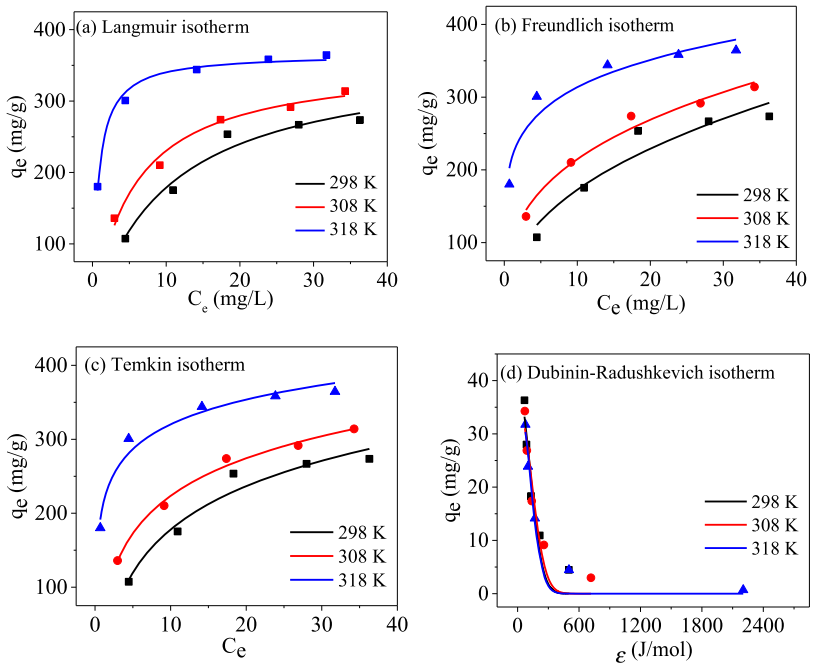

Figure 12. Fitting results of adsorption isotherms with PPy-PANI/M-SBA-5 at 298, 308, and 318 K. Langmuir (a), Freundlich (b), Temkin (c), and Dubinin−Radushkevich (d).

experiment investigated the adsorption of mercury ions onto the PPy-PANI/M-SBA-15 adsorbent with the contact time. It can be seen from Figure 11a that the time required for the adsorption to reach equilibrium is approximately 360 min.

In the early stage of the experiment, the adsorption efficiency of the adsorbent is very fast, and the adsorption capacity reaches 159.6 mg/g at 30 min. This is because there are enough adsorption sites in the initial stage. As the process progresses, the available adsorption sites are gradually reduced until the adsorption equilibrium is reached at 360 min.[39]

With the purpose to find out the mechanism as the main limiting step in the adsorption process, different kinetic models have been used to evaluate experimental data. Usually, the Lagergren model (eq 4), the pseudo-second-order model (eq 5), and the Elovich dynamic model (eq 6) are used to fit the kinetic data, and the corresponding chart data are listed in Figure 11b and Table S1 (Supporting Information).

$$q_t = \left(1 - \frac{1}{e^{k_1 t}}\right) q_e \tag{4}$$

$$q_t = \frac{k_2 t q_e^2}{1 + k_t t q_e} \tag{5}$$

https://doi.org/10.1021/acsomega.1c04249
ACS Omega 2021, 6, 25791−25806

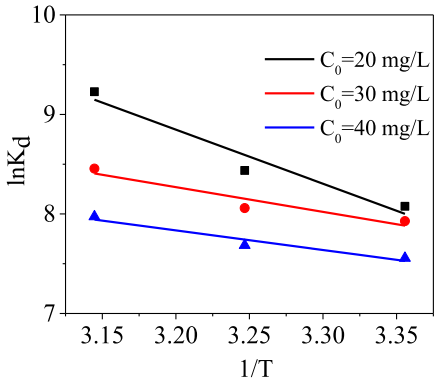

Figure 13. Thermodynamic fitting of mercury adsorption by PPy-PANI/M-SBA-15.

$$q_t = \beta \ln(\alpha\beta) + \beta \ln t \quad (6)$$

where q_t (mg/g) refers to the amount of adsorbates adsorbed per unit of the adsorbent at time t (min) and k_1 and k_2 are the Lagergren and pseudo-second-order rate constants, respectively.

From the data in Figure 11b and Table S1, it can be concluded that the pseudo-second-order model (R^2 = 0.9309) has a higher degree of fitting for PPy-PANI/M-SBA-15 than the Lagergren model (R^2 = 0.8580). The result shows that the chemical action in the adsorption process is the main part, not the mass transfer, and that the pseudo-second-order kinetic model is more suitable for the adsorption process of this experiment.[29] In addition, the calculated capacity of the pseudo-second-order kinetic model $q_{e,cal}$ of 241.5 mg/g is closer to the experimental value $q_{e,exp}$ of 253.8 mg/g. which also supports the above conclusions.

The Elovich kinetic model proposes that the surface of the adsorbent is heterogeneous, and the adsorption kinetics has an effect on the desorption or interaction between the PPy-PANI/M-SBA-15 and Hg(II) ions. It has been shown to be effective in describing the interaction between the solid and liquid. From Table S1, the value of β expressed as the desorption coefficient can be obtained from 0.3 to 0.9, which indicates that the desorption rate is low.[31] The high correlation coefficient (R^2 = 0.9924) proves that the adsorption system is controlled by the chemisorption process and is consistent with the fitting results of the pseudo-second-order kinetic model.

Generally, the rate-limiting step can be a single step or a combination of diffusion steps. It can be fitted according to the Weber−Morris model, and the relevant formula is as shown in eq 7. The data graph of q_t versus $t^{1/2}$ is depicted to predict the rate-limiting step:

$$q_t = k_{d-i} t^{1/2} + C_i \quad (7)$$

Among them, K_{d-i} (mg/(g min$^{0.5}$)) is the intraparticle rate constant. It can be seen from Figure 11c that the adsorption of Hg(II) ions undergoes a rapid adsorption phase, followed by a decrease in the diffusion rate and finally reaches an equilibrium, which can be divided into three stages over the entire time range. The first stage is the instantaneous adsorption, which describes the mass transfer of Hg(II) ions from the bulk solution to the outer surface of PPy-PANI/M-SBA-15 by diffusion. The second stage is the gradual adsorption zone dominated by intraparticle diffusion. The last stage is due to the reduction of the remaining Hg(II) ions in the solution and the active sites available for adsorption, resulting in a slow diffusion rate until the adsorption equilibrium.[40]

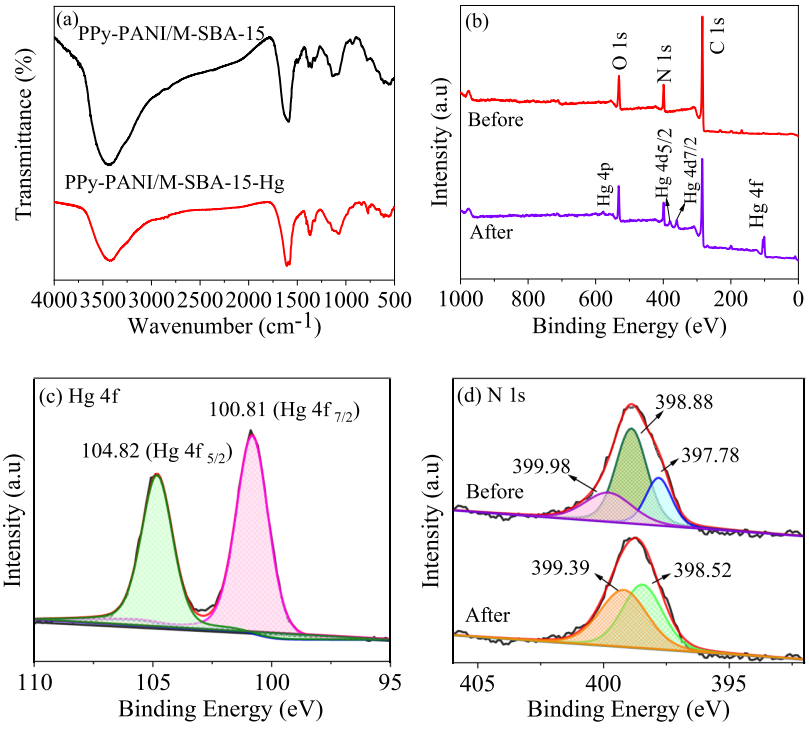

Figure 14. FT-IR spectra of PPy-PANI/M-SBA-15 before and after adsorption (a), XPS spectra of wide scan (b), Hg 4f after adsorption (c), N 1s spectra of PPy-PANI/M-SBA-15 before and after adsorption (d).

https://doi.org/10.1021/acsomega.1c04249
ACS Omega 2021, 6, 25791−25806

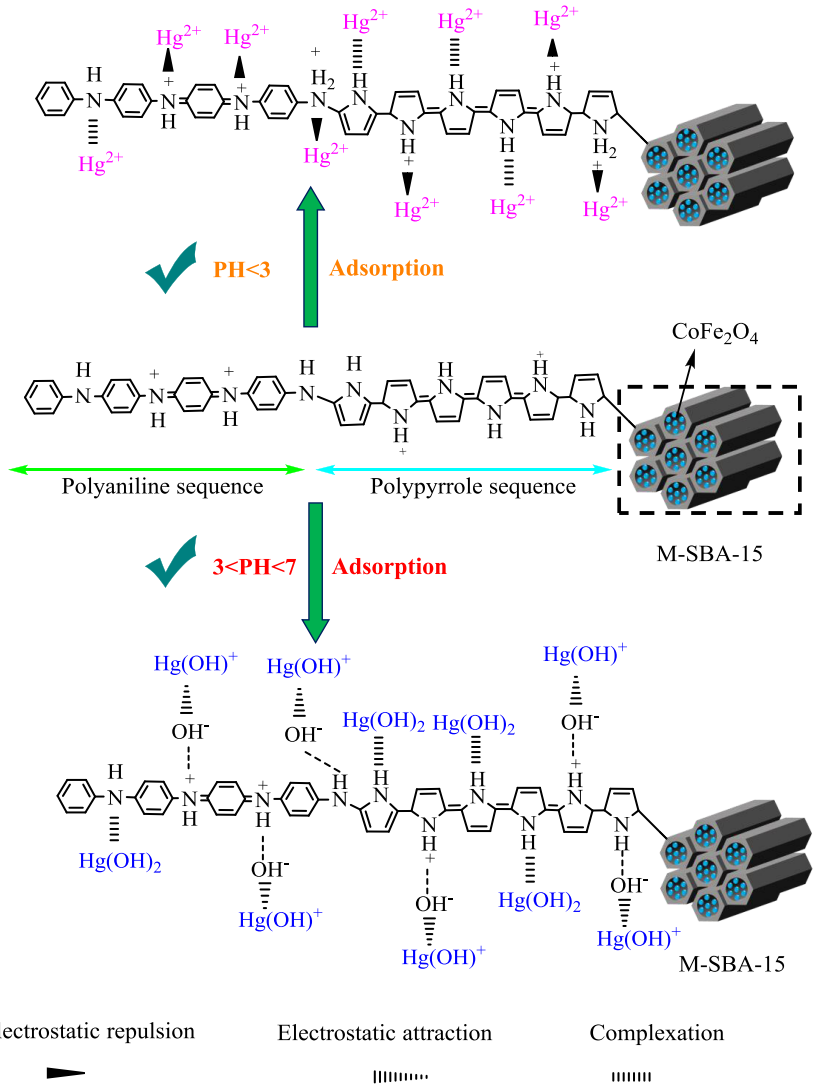

Figure 15. Possible mechanism of adsorption of mercury ions onto PPy-PANI/M-SBA-15.

According to the correlation coefficient listed in Table S1, the order of $k_{d\text{-}1} > k_{d\text{-}2} > k_{d\text{-}3}$ can be obtained, so it can be concluded that the whole adsorption process is mainly controlled by the first stage and the second stage. If the plotted linear graph of q_t versus $t^{1/2}$ does not pass the far point, it means that the intraparticle diffusion is not the only rate-determining step.[41]

3.4. Isotherm Experiments. The study of adsorption isotherms not only plays an important role in describing the adsorption of PPy-PANI/M-SBA-15 on Hg(II) ions and understanding the balance between the two but also has guiding significance for the large-scale application of PPy-PANI/M-SBA-15.[42] Therefore, the adsorption isotherm experiments of the adsorbent PPy-PANI/M-SBA-15 on Hg(II) ions were carried out at three different temperatures of 298, 308, and 318 K to derive the most suitable isotherm of the four isotherm models of Langmuir (eq 8), Freundlich (eq 9), Temkin (eq 10), and Dubinin–Radushkevich (eq 11). The fitted models and corresponding data are listed in Figure 12 and Table S2, respectively.

$$q_e = \frac{Q_m K_L C_e}{1 + K_L C_e} \tag{8}$$

$$q_e = K_F C_e^{1/n} \tag{9}$$

$$q_e = \frac{RT}{b_T} \ln(K_T C_e) \tag{10}$$

$$q_e = q_{max} \exp(-\beta \varepsilon^2) \tag{11}$$

$$R_L = \frac{1}{1 + K_L C_0} \tag{12}$$

Here, Q_m (mg/g) is the maximum adsorption capacity, K_L (L/mg) is the Langmuir constant related to the adsorption energy, and K_F and n are the Freundlich constants, related to the adsorption capacity and adsorption strength, respectively. It is worth noting that the small "$1/n$" value indicates a strong interaction between the adsorbents and the adsorbates. b_T is the Temkin constant associated with the heat of adsorption and K_T is the isotherm constant.

The fitted maps for the Langmuir and Freundlich models are given in Figure 12a,b, and the corresponding data are listed in Table S2. It can be seen that the Langmuir model is more suitable for the adsorption process of this study than the Freundlich model. This result is supported by a high R^2 value

https://doi.org/10.1021/acsomega.1c04249
ACS Omega 2021, 6, 25791−25806

and a low x^2, SSE, and RMSE values and good agreement between the experimental maximum adsorption capacity and the corresponding calculated value of the isotherm.

The Langmuir model is based on the assumption of monolayer and homogeneous chemisorption, indicating that the PPy-PANI/M-SBA-15 mainly uses chemical adsorption to remove Hg(II) ions. There is no interaction between the adsorbed Hg(II) ions. The feasibility of the adsorption process is usually judged based on the equilibrium parameter R_L (eq 12). The obtained data R_L is between 0 and 1, indicating that chemisorption is advantageous.[43]

Meantime, it is worth noting that the Q_m value decreases with increasing temperature, and the R_L value increases, reflecting the exothermic nature of the adsorption process. Meanwhile, the maximum adsorption capacity Q_m of the fitting can reach 363.9 mg/g at 298 K, indicating that the prepared PPy-PANI/M-SBA-15 material has a higher adsorption capacity than many other functionalized mesoporous materials.[34,37,44]

The Temkin model (Figure 12c) assumes the linear relationship between the adsorption heat and temperature, taking into account the effect of temperature on the isotherm. As can be seen from Table S2, the Temkin isotherm also has a high R^2 value (0.9574−0.9922) and a low x^2 value (0.9431−0.9896), SSE value (162.4−885.1) and RMSE value (7.36−17.18). In all cases, a relatively high K_T value indicates a high potential combination between PPy-PANI/M-SBA-15 and Hg(II) ions. At high temperatures, a larger b_T value reveals that an increase in temperature promotes the interaction between PPy-PANI/M-SBA-15 and Hg(II) ions.

The Dubinin−Radushkevich (D−R) adsorption isotherm model (Figure 12d) considers that ionic species are first combined with the most favorable sites of energy and are widely used to calculate the average adsorption energy per mole of metal ions transferred from the liquid phase to the surface of the adsorbent (E, kJ/mol). The value of E can be obtained by the following equation (eq 13)

$$E = \frac{1}{(2\beta)^{1/2}} \tag{13}$$

The magnitude of the E value can be used to distinguish the type of adsorption process of PPy-PANI/M-SBA-15 for mercury ions. The adsorption process at $E < 8$ kJ/mol is a physical property, and at $E > 16$ kJ/mol, it can be explained by a chemisorption mechanism. The E values obtained in Table S2 are all greater than 16 kJ/mol, indicating that the adsorption of this experiment is controlled by chemisorption.[44] According to the data in Table S2, it can be seen that q_{max} obtained at a high temperature is not large, revealing the exothermic nature of the adsorption process, which is consistent with the conclusion obtained by the Langmuir model.

Furthermore, to evaluate the performance of PPy-PANI/M-SBA-15, the performance of PPy-PANI/M-SBA-15 was compared with many other adsorptive materials, and the results are shown in Table S3 (SI). From Table S3, it can be seen that the adsorption capacity of PPy-PANI/M-SBA-15 is far higher than those of many other adsorptive materials. The results show that PPy-PANI/M-SBA-15 is a promising adsorbent in the application of wastewater treatment.

In addition, the recycle experiment is also shown in the SI. As shown in Figure S2, the adsorption of PPy-PANI/M-SBA-15 still reaches over 150 mg/g after five cycles, which indicates that the as-prepared PPy-PANI/M-SBA-15 has good reproducibility performance.

3.5. Thermodynamic Experiment. The properties and mechanisms of the adsorption process can be analyzed by thermodynamic analysis. The values of ΔG°, ΔH°, and ΔS° are calculated by eqs 14 and 15 and are used to describe the thermodynamic behavior of the adsorbent

$$\Delta G^0 = -RT \ln K_d \tag{14}$$

$$\ln K_d = \frac{\Delta S^0}{R} - \frac{\Delta H^0}{RT} \tag{15}$$

In that, ΔH° and ΔS° are obtained according to the slope and intercept of the plotted form of $\ln K_d$ and $1/T$, respectively. The thermodynamic parameters obtained are listed in Table S4 and the fitting results are shown in Figure 13. The negative ΔG° value confirms that the adsorption of PPy-PANI/M-SBA-15 toward Hg(II) ions is a spontaneous behavior.[45] The values of ΔG° are all less than −40 kJ/mol, indicating that the adsorption of mercury ions by PPy-PANI/M-SBA-15 belongs to the chemical adsorption category.[46]

However, the positive value of ΔH° reflects an endothermic property, which is consistent with the results obtained by the Langmuir model and the D−R model.[47] The positive value of ΔS° for mercury ions reveals that the increase of the randomness in the interface of the solid/solution and a high temperature is favorable for the adsorption of Hg(II).[41,48]

3.6. Mechanism Speculation. To investigate whether the performance of PPy-PANI/M-SBA-15 changes before and after adsorption, an FT-IR test was performed.

As shown in Figure 14a, the FT-IR spectrum of PPy-PANI/M-SBA-15 before and after adsorption shows that the intensity of each characteristic peak is reduced, which reveals that the reduction of nitrogen-containing functional groups in various forms can be explained as the combination of nitrogen-containing functional groups and mercury ions to form complexes.[49]

A wide range and high-resolution scanning of key elements was studied to gain insight into the adsorption mechanism of the new material to remove mercury ions from aqueous solutions. As shown in Figure 14b, it can be clearly seen from the used PPy-PANI/M-SBA-15 that the presence of Hg 4f confirms that the Hg(II) ions are successfully adsorbed by the PPy-PANI/M-SBA-15. The binding energies of Hg $4f_{7/2}$ and Hg $4f_{5/2}$ are 100.81 and 104.82 eV, respectively (Δ = 4.01 eV) (Figure 14c). Comparing the binding energy of Hg(II) ions measured in this experiment with the values in ref 2, it is known that the adsorbed mercury ions exist in the form of divalent mercury ions (Hg(II)), indicating that adsorbed Hg(II) does not undergo the redox reaction on PPy-PANI/M-SBA-15.

For the PPy-PANI/M-SBA-15 composite, since both polypyrrole and polyaniline have nitrogen-containing functional groups in the main chain, the adsorption selectivity of the two polymer bodies is uniform. After polymerization occurs, an amino group that adsorbs mercury ions is formed on both polymer backbones. To further obtain the adsorption mechanism of mercury ions by copolymers of pyrrole and aniline, XPS analysis of N elements before and after adsorption was carried out. It can be seen from Figure 14d that there are three forms of the N element before adsorption in the spectrogram, including anthraquinone imine (=N−), benzene amine (−NH−), and electronic state-doped imine ($-NH^+-$).

https://doi.org/10.1021/acsomega.1c04249
ACS Omega 2021, 6, 25791−25806

Since at a low pH (less than 3), protonation occurs as a chemically active amino group such that the nitrogen atom has a lone pair of electrons. To maintain charge neutrality, more anions are required to enter, in which case causes an undesirable adsorption effect. However, with the gradual increase of the pH value, the amino group completes the process of deprotonation. Meanwhile, the nitrogen atom with the lone pair of electrons in the macromolecular chain of the copolymer becomes the main adsorption site, and mercury ions can share a lone pair of electrons with a nitrogen atom to form a stable metal complex.[26]

Simultaneously, the presence of mercury ions is also strongly related to the pH of the solution. At high pH values (3−7), mercury ions mainly exist in the form of $Hg(OH)_2$, which has a larger size and faster migration rate, which makes the adsorption effect better.[8,37] It is also based on the characteristics of amino and metal mercury ions. In this experiment, various factors were investigated under the condition of pH = 7.

Subsequently, comparing the X-ray spectrum of the N element before adsorption, it is found that there are only the two forms of quinone imine (=N−) and benzene amine (−NH−) in the peak fitting map of the N element after adsorption. The position of the characteristic peak is also shifted from 397.52 and 398.88 eV to 398.52 and 399.39 eV, respectively. The shift proves that the amino group on the copolymer is complexed with mercury ions.[50] The chemically active amino group forms a stable metal complex with mercury ions, i.e., N−Hg, thereby achieving the removal of mercury ions from aqueous solution. The adsorption mechanism is mainly a complex reaction and electrostatic attraction. On this basis, a possible adsorption mechanism diagram of PPy-PANI/M-SBA-15 for the removal of heavy metal mercury ions is proposed (Figure 15). In addition, the matrix short-channel SBA-15 of PPy-PANI/M-SBA-15 also contributes to the adsorption of mercury ions to some extent.

4. CONCLUSIONS

In this paper, a novel composite adsorbent of pyrrole and aniline copolymer-modified magnetic short-channel mesoporous silica SBA-15 was synthesized, and the influence of various factors on the removal of mercury ions in aqueous solution was investigated. The experimental data and RSM results indicate that the maximum adsorption capacity of PPy-PANI/M-SBA-15 can reach 346.2 mg/g under the optimal conditions of 6.7, temperature of 310 K, C_0 of 29.5 mg/L, and dosage of 0.044 g/L. The adsorption of mercury ions onto PPy-PANI/M-SBA-15 conforms to the pseudo-second-order kinetic and Langmuir models. The fitting of Temkin and thermodynamic models shows that the adsorption reaction is spontaneous and endothermic. The E value calculated by the D−R model shows that the adsorbent process belongs to the category of chemical adsorption. The results of XPS analysis indicate that a stable metal complex resulted from the covalent bond between the nitrogen-containing functional groups, and mercury ions are the main removal method for Hg(II) ions. In addition, excellent magnetic properties and high reproducibility exhibit that PPy-PANI/M-SBA-15 has excellent recyclability and environmentally friendly properties and can be a potential heavy metal ion adsorbent in practical applications.

■ ASSOCIATED CONTENT

Supporting Information

The Supporting Information is available free of charge at https://pubs.acs.org/doi/10.1021/acsomega.1c04249.

EDS spectrum and EDX elemental mapping of PPy-PANI/M-SBA-15 (Figure S1); regeneration performance of PPy-PANI/M-SBA-15 (Figure S2); kinetic fitting for adsorption of Hg(II) onto PPy-PANI/M-SBA-15 (Table S1); adsorption isotherm parameters of PPy-PANI/M-SBA-15 (Table S2); comparison of the adsorption capacity for mercury(II) ions (Table S3); and thermodynamic parameters of adsorption of mercury by PPy-PANI/M-SBA-15 (Table S4) (PDF)

■ AUTHOR INFORMATION

Corresponding Author

Yongfu Guo − *School of Environmental Science and Engineering, Suzhou University of Science and Technology, Suzhou 215009, China; Jiangsu Collaborative Innovation Center of Technology and Material of Water Treatment, Suzhou University of Science and Technology, Suzhou 215009, China;* orcid.org/0000-0002-2562-865X; Phone: +86 512 68092987; Email: yongfuguo@163.com

Authors

Jingtao Shen − *School of Environmental Science and Engineering, Suzhou University of Science and Technology, Suzhou 215009, China*

Shuyuan Zhang − *School of Environmental Science and Engineering, Suzhou University of Science and Technology, Suzhou 215009, China*

Zheng Zeng − *School of Environmental Science and Engineering, Suzhou University of Science and Technology, Suzhou 215009, China*

Jialun Huang − *School of Environmental Science and Engineering, Suzhou University of Science and Technology, Suzhou 215009, China*

Yi Shen − *School of Environmental Science and Engineering, Suzhou University of Science and Technology, Suzhou 215009, China*

Complete contact information is available at: https://pubs.acs.org/10.1021/acsomega.1c04249

Author Contributions

§J.S. and S.Z. contributed equally to this work.

Notes

The authors declare no competing financial interest.

■ ACKNOWLEDGMENTS

This work was supported by the National Natural Science Foundation of China (No. 51578354), Suzhou Science and Technology Bureau (SS201802), Natural Science Research Project of Jiangsu Province Higher Education (18KJA610002), and Research Innovation Project for College Graduates of Jiangsu Province (KYCX21_3023, CYCX21_3037). In addition, the authors would like to acknowledge Shiyanjia Lab (www.shiyanjia.com).

■ REFERENCES

(1) Mudasir, M.; Baskara, R. A.; Suratman, A.; Yunita, K. S.; Perdana, R.; Puspitasari, W. Simultaneous adsorption of Zn(II) and Hg(II) ions on selective adsorbent of dithizone-immobilized

bentonite in the presence of Mg(II) ion. *J. Environ. Chem. Eng.* **2020**, *8*, No. 104002.
(2) Das, R.; Giri, S.; Muliwa, A. M.; Maity, A. High-performance Hg(II) removal using thiol-functionalized polypyrrole (PPy/MAA) composite and effective catalytic activity of Hg(II) adsorbed waste material. *ACS Sustainable Chem. Eng.* **2017**, *5*, 7524−7536.
(3) Wang, X.; Zhang, Z.; Zhao, Y.; Xia, K.; Guo, Y.; Qu, Z.; Bai, R. A mild and facile synthesis of amino functionalized $CoFe_2O_4$@SiO_2 for Hg(II) removal. *Nanomaterials* **2018**, *8*, No. 673.
(4) Chen, S.-Y.; Lee, J.-F.; Cheng, S. Pinacol-type rearrangement catalyzed by Zr-incorporated SBA-15. *J. Catal.* **2010**, *270*, 196−205.
(5) Xie, Y.; Yan, B.; Tian, C.; Liu, Y.; Liu, Q.; Zeng, H. Efficient removal of elemental mercury (Hg) by SBA-15-Ag adsorbents. *J. Mater. Chem. A* **2014**, *2*, 17730−17734.
(6) Shen, Y.; Jiang, N.; Liu, S.; Zheng, C.; Wang, X.; Huang, T.; Guo, Y.; Bai, R. Thiol functionalization of short channel SBA-15 through a safe, mild and facile method and application for the removal of mercury (II). *J. Environ. Chem. Eng.* **2018**, *6*, 5420−5433.
(7) Fan, Q.; Yang, Y.; Hao, Y.; Zhao, X.; Feng, Y. Preparation of three-dimensional PANI/GO for the separation of Hg(II) from aqueous solution. *J. Mol. Liq.* **2015**, *212*, 557−562.
(8) Li, R.; Liu, L.; Yang, F. Removal of aqueous Hg(II) and Cr(VI) using phytic acid doped polyaniline/cellulose acetate composite membrane. *J. Hazard. Mater.* **2014**, *280*, 20−30.
(9) Ballav, N.; Das, R.; Giri, S.; Muliwa, A. M.; Pillay, K.; Maity, A. L-cysteine doped polypyrrole (PPy@L-Cyst): A super adsorbent for the rapid removal of Hg^{2+} and efficient catalytic activity of the spent adsorbent for reuse. *Chem. Eng. J.* **2018**, *345*, 621−630.
(10) Huang, Y.; Li, J.; Chen, X.; Wang, X. Applications of conjugated polymer based composites in wastewater purification. *RSC Adv.* **2014**, *4*, 62160−62178.
(11) Tabit, R.; Amadine, O.; Essamlali, Y.; Ĥanoun, K.; Rhihila, A.; Zahouily, M. Magnetic $CoFe_2O_4$ nanoparticles supported on graphene oxide ($CoFe_2O_4$/GO) with high catalytic activity for peroxymonosulfate activation and degradation of rhodamine B. *RSC Adv.* **2018**, *8*, 1351−1360.
(12) Yan, X.; Chen, J.; Xue, Q.; Miele, P. Synthesis and magnetic properties of $CoFe_2O_4$ nanoparticles confined within mesoporous silica. *Microporous Mesoporous Mater.* **2010**, *135*, 137−142.
(13) Dash, S.; Chaudhuri, H.; Gupta, R.; Nair, U. G.; Sarkar, A. Fabrication and application of low-cost thiol functionalized coal fly ash for selective adsorption of heavy toxic metal ions from water. *Ind. Eng. Chem. Res.* **2017**, *56*, 1461−1470.
(14) Zhu, H.; Shen, Y.; Wang, Q.; Chen, K.; Wang, X.; Zhang, G.; Yang, J.; Guo, Y.; Bai, R. Highly promoted removal of Hg(II) with magnetic $CoFe_2O_4$@SiO_2 core−shell nanoparticles modified by thiol groups. *RSC Adv.* **2017**, *7*, 39204−39215.
(15) Wang, X.; Chen, M.; Li, L.; Jin, D.; Jin, H.; Ge, H. Magnetic properties of SBA-15 mesoporous nanocomposites with $CoFe_2O_4$ nanoparticles. *Mater. Lett.* **2010**, *64*, 708−710.
(16) Wang, H.; Huang, J.; Ding, L.; Li, D.; Han, Y. A facile synthesis of monodisperse $CoFe_2O_4$/SiO_2 nanoparticles. *Appl. Surf. Sci.* **2011**, *257*, 7107−7112.
(17) Wang, F.; Li, J.; Yuan, J.; Sun, X.; Shen, J.; Han, W.; Wang, L. Short channeled Zr-Ce-SBA-15 supported palladium catalysts for toluene catalytic oxidation. *Catal. Commun.* **2011**, *12*, 1415−1419.
(18) Chen, X.; Wang, P.; Xu, J.; Han, Y.; Jin, H.; Jin, D.; Peng, X.; Hong, B.; Li, J.; Yang, Y.; Ge, H.; Wang, X. Magnetic separation and adsorptive performance for methylene blue of mesoporous $NiFe_2O_4$/SBA-15 nanocomposites. *Adv. Powder Technol.* **2017**, *28*, 2087−2093.
(19) Singh, C.; Goyal, A.; Bansal, S.; Singhal, S. SiO_2@MFe_2O_4core-shell nanostructures: Efficient photocatalysts with excellent dispersion properties. *Mater. Res. Bull.* **2017**, *85*, 109−120.
(20) Molamahmood, H. V.; Ebadi, T.; Eskandari, R. Adsorption of mercury by polyaniline/polyvinyl alcohol in an aqueous environment. *Water, Air, Soil Pollut.* **2018**, *229*, 1−9.
(21) He, K.; Qin, C.; Wen, Q.; Wang, C.; Wang, B.; Yu, S.; Hao, C.; Chen, K. Facile fabrication of polyaniline/polypyrrole copolymer nanofibers with a rough surface and their electrorheological activities. *J. Appl. Polym. Sci* **2018**, *135*, No. 6289.
(22) Salahi, S.; lashkenari, M. S.; Abbaszadeh, M.; Pousti, M.; Ghorbani, M. Synthesis and representation of a new structure for polypyrrole−chitosan nanocomposite and investigation of effect of intermolecular interaction. *Synth. Met.* **2014**, *197*, 154−158.
(23) Lim, C. W.; Song, K.; Kim, S. H. Synthesis of PPy/silica nanocomposites with cratered surfaces and their application in heavy metal extraction. *J. Ind. Eng. Chem.* **2012**, *5*, 24−28.
(24) Bhaumik, M.; McCrindle, R.; Maity, A. Efficient removal of congo red from aqueous solutions by adsorption onto interconnected polypyrrole−polyaniline nanofibres. *Chem. Eng. J.* **2013**, *228*, 506−515.
(25) Xu, P.; Han, X.; Wang, C.; Zhang, B.; Wang, X.; Wang, H.-L. Facile synthesis of polyaniline-polypyrrole nanofibers for application in chemical deposition of metal nanoparticlesa. *Macromol. Rapid Commun.* **2008**, *29*, 1392−1397.
(26) Li, R.; Liu, L.; Yang, F. Polyaniline/reduced graphene oxide/Fe_3O_4 nano-composite for aqueous Hg(II) removal. *Water Sci. Technol.* **2015**, *72*, 2062−2070.
(27) Kera, N. H.; Bhaumik, M.; Pillay, K.; Ray, S. S.; Maity, A. Selective removal of toxic Cr(VI) from aqueous solution by adsorption combined with reduction at a magnetic nanocomposite surface. *J. Colloid Interface Sci.* **2017**, *503*, 214−228.
(28) Zhou, Z.; Hao, T.; Xia, L.; Nie, Y.; Li, S. Preparation of a novel magnetic and thermo-responsive composite and its application in drug release. *Monatsh. Chem.* **2017**, *148*, 1205−1213.
(29) Aghajani, K.; Tayebi, H.-A. Synthesis of SBA-15/PAni mesoporous composite for adsorption of reactive dye from aqueous media: RBF and MLP networks predicting models. *Fibers Polym.* **2017**, *18*, 465−475.
(30) Javadian, H.; Taghavi, M. Application of novel Polypyrrole/thiol-functionalized zeolite Beta/MCM-41 type mesoporous silica nanocomposite for adsorption of Hg^{2+} from aqueous solution and industrial wastewater: Kinetic, isotherm and thermodynamic studies. *Appl. Surf. Sci.* **2014**, *289*, 487−494.
(31) Shafiabadi, M.; Dashti, A.; Tayebi, H.-A. Removal of Hg (II) from aqueous solution using polypyrrole/SBA-15 nanocomposite: Experimental and modeling. *Synth. Met.* **2016**, *212*, 154−160.
(32) Cao, T.; Wang, C.; Zhou, Z.; Liu, L.; Xu, S.; Song, H.; Lin, W.; Xu, Z. Magnetic multi-functional SBA-15 supported silver nanocomposites: Synthesis, characterization and application. *Appl. Surf. Sci.* **2021**, *552*, No. 149787.
(33) Chen, L.; Zhao, D.; Chen, S.; Wang, X.; Chen, C. One-step fabrication of amino functionalized magnetic graphene oxide composite for uranium(VI) removal. *J. Colloid Interface Sci.* **2016**, *472*, 99−107.
(34) Lin, Z.; Pan, Z.; Zhao, Y.; Qian, L.; Shen, J.; Xia, K.; Guo, Y.; Qu, Z. Removal of Hg^{2+} with polypyrrole-functionalized Fe_3O_4/Kaolin: Synthesis, performance and optimization with response surface methodology. *Nanomaterials* **2020**, *10*, No. 1370.
(35) Anbia, M.; Lashgari, M. Synthesis of amino-modified ordered mesoporous silica as a new nano sorbent for the removal of chlorophenols from aqueous media. *Chem. Eng. J.* **2009**, *150*, 555−560.
(36) Asfaram, A.; Ghaedi, M.; Agarwal, S.; Tyagi, I.; Kumar Gupta, V. Removal of basic dye auramine-O by ZnS:Cu nanoparticles loaded on activated carbon: optimization of parameters using response surface methodology with central composite design. *RSC Adv.* **2015**, *5*, 18438−18450.
(37) Zhang, Z.; Xia, K.; Pan, Z.; Yang, C.; Wang, X.; Zhang, G.; Guo, Y.; Bai, R. Removal of mercury by magnetic nanomaterial with bifunctional groups and core-shell structure: Synthesis, characterization and optimization of adsorption parameters. *Appl. Surf. Sci.* **2020**, *500*, No. 143970.
(38) Shitanshu Pandey, S. K. Reactive extraction of gallic acid from aqueous solution with Tri-noctylamine in oleyl alcohol: Equilibrium, thermodynamics and optimization using RSM-rCCD. *Sep. Purif. Technol.* **2020**, *231*, No. 115904.

https://doi.org/10.1021/acsomega.1c04249
ACS Omega 2021, 6, 25791−25806

(39) Kong, J.; Gu, R.; Yuan, J.; Liu, W.; Wu, J.; Fei, Z.; Yue, Q. Adsorption behavior of Ni(II) onto activated carbons from hide waste and high-pressure steaming hide waste. *Ecotoxicol. Environ. Saf.* **2018**, *156*, 294−300.
(40) Zhang, X.; Jiao, C.; Wang, J.; Liu, Q.; Li, R.; Yang, P.; Zhang, M. Removal of uranium(VI) from aqueous solutions by magnetic schiff base: Kinetic and thermodynamic investigation. *Chem. Eng. J.* **2012**, *198−199*, 412−419.
(41) Dindar, M. H.; Yaftian, M. R.; Rostamnia, S. Potential of functionalized SBA-15 mesoporous materials for decontamination of water solutions from Cr(VI), As(V) and Hg(II) ions. *J. Environ. Chem. Eng.* **2015**, *3*, 986−995.
(42) Boujaady, H. E.; Mourabet, M.; Bennani-Ziatni, M.; Taitai, A. Adsorption/desorption of direct yellow 28 on apatitic phosphate: Mechanism, kinetic and thermodynamic studies. *J. Assoc. Arab Univ. Basic Appl. Sci.* **2014**, *16*, 64−73.
(43) Ren, Y.; Abbood, H. A.; He, F.; Peng, H.; Huang, K. Magnetic EDTA-modified chitosan/SiO_2/Fe_3O_4 adsorbent: Preparation, characterization, and application in heavy metal adsorption. *Chem. Eng. J.* **2013**, *226*, 300−311.
(44) Xia, K.; Guo, Y.; Shao, Q.; Zan, Q.; Bai, R. Removal of mercury (II) by EDTA-functionalized magnetic $CoFe_2O_4$@SiO_2 nanomaterial with core-shell structure. *Nanomaterials* **2019**, *9*, No. 1532.
(45) Zhang, Y.; Li, Q.; Sun, L.; Tang, R.; Zhai, J. High efficient removal of mercury from aqueous solution by polyaniline/humic acid nanocomposite. *J. Hazard. Mater.* **2010**, *175*, 404−409.
(46) Salahi, S.; Parvini, M.; Ghorbani, M. Equilibrium studies in adsorption of Hg(II) from aqueous solutions using biocompatible polymeric polypyrrole-chitosan nanocomposite. *Polycyclic Aromat. Compd.* **2014**, *34*, 225−236.
(47) Tang, R.; Li, Q.; Cui, H.; Zhang, Y.; Zhai, J. Adsorption of aqueous Hg (II) by a novel poly (aniline-co-o-aminophenol)/mesoporous silica SBA-15 composite. *Polym. Adv. Technol.* **2010**, *6*, 2231−2236.
(48) Zhao, Y.; Xia, K.; Zhang, Z.; Zhu, Z.; Guo, Y.; Qu, Z. Facile synthesis of polypyrrole-functionalized $CoFe_2O_4$@SiO_2 for removal for Hg(II). *Nanomaterials* **2019**, *9*, No. 455.
(49) Gupta, V. K.; Nayak, A.; Agarwal, S.; Tyagi, I. Potential of activated carbon from waste rubber tire for the adsorption of phenolics: Effect of pre-treatment conditions. *J. Colloid Interface Sci.* **2014**, *417*, 420−30.
(50) Pan, S.; Zhang, Y.; Shen, H.; Hu, M. An intensive study on the magnetic effect of mercapto-functionalized nano-magnetic Fe_3O_4 polymers and their adsorption mechanism for the removal of Hg(II) from aqueous solution. *Chem. Eng. J.* **2012**, *210*, 564−574.

https://doi.org/10.1021/acsomega.1c04249
ACS Omega 2021, 6, 25791−25806